Electron energy-loss spectroscopy of the O *K* edge of NbO_2, MoO_2, and WO_2

Nan Jiang and John C. H. Spence
Department of Physics and Astronomy, Arizona State University, Tempe, Arizona 852870-1504, USA
(Received 21 June 2004; published 21 December 2004)

Experimental high-energy transmission electron energy-loss absorption spectra from the oxygen *K* edges of NbO_2, MoO_2, and WO_2 are compared with electronic structure calculations for the relevant empty states, based on the linear augmented plane wave (plus local orbital) method, in the local density approximation. These are also compared with calculations for an idealized rutile structure. The agreement of these ground-state density functional theory calculations (without core-hole effects) for these transition metal dioxides at our resolution of about 1 eV is excellent, and shows in each case an underlying structure consisting of five main peaks, despite differences in local atomic and electronic structure. We find also that shoulderlike features on an e_g peak can be related to structural distortions induced by the formation of metal-metal bonds.

DOI: 10.1103/PhysRevB.70.245117 PACS number(s): 79.20.Uv, 71.15.Mb, 71.20.Ps

I. INTRODUCTION

Transition metal dioxides (MO_2) have a variety of interesting physical properties.[1] One particular interesting phenomenon is that these dioxides show a wide range of electrical conductivity: from insulators (e.g., TiO_2) to semiconductors (e.g., NbO_2) to conductors (e.g., MoO_2 and WO_2). Some exhibit temperature-induced metal-insulator transitions (e.g., VO_2 and NbO_2). From an atomic structure point of view, most of the transition metal dioxides have crystal structures related to tetragonal rutile TiO_2.[2] From an electronic structure point of view, the transition metals that form dioxides with rutile-related structures have incompletely filled *d* shells. Many of their physical properties (in particular, electrical conductivity) are attributable to *d* electron behavior. However, whether the mechanism can be explained using one-electron band theory[3] or requires strong electron-electron correlation[4,5] is still unknown. However, recent calculations of band structure using density functional theory (DFT) in the local density approximation (LDA) favor the former.[6–8] In support of the band theory calculations, experimental data on the occupied and unoccupied electronic density of states (DOS) are needed. In this work, we investigate the unoccupied DOS for NbO_2, MoO_2, and WO_2 by measuring electron energy-loss spectra (EELS) at the oxygen *K* edge.

The occupied DOS of NbO_2 and MoO_2 have so far been largely studied based on optical, ultraviolet photoelectron (UPS), x-ray photoelectron (XPS), and x-ray emission (XES) spectroscopy experiments.[9,10] No measurements of the unoccupied DOS of these dioxides have been reported. In EELS, we detect a fraction of a high-energy beam of electrons which, on traversing a thin slab, has lost energy by excitation of a core electron from an initial state to an unoccupied final state. By analogy with x-ray absorption, the transition probabilities for EELS can be calculated using Fermi's golden rule, and the energy-loss near-edge fine structure (ELNES) is then determined by the density of final states, projected onto the excited atom's crystal site and symmetry.[11] Since it is restricted by the dipole selection rule, for example, the O *K* ELNES probes the unoccupied oxygen *p* DOS, assuming that the atomic background varies slowly with energy, and that core-hole effects have been efficiently screened by valence electrons. In this work, the interpretation of the O *K* ELNES was obtained by comparison with band theory calculations. The consistency between experiment and simulations establishes the accuracy of our band theory calculations.

II. EXPERIMENT

NbO_2, MoO_2, and WO_2 crystals (Alfa Aesar) were used in this study. The crystal structure was confirmed by x-ray diffraction. No impurities were apparent in the energy dispersive characteristic x-ray spectra. The transmission electron microscope (TEM) samples were prepared by grinding the oxides into powders in acetone, and picking them up using a Cu grid covered with a lacy carbon film. The samples were then immediately transferred into a Philips EM400 TEM with a field-emission gun operating at 100 keV, and a Gatan parallel EELS system. The energy resolution of the energy-loss spectrometer is about 1.0 eV [determined by the full width at half maximum (FWHM) of the zero-loss peak]. The collection semiangle is about 5 mrad. To reduce the noise from channel-to-channel gain variations of the photodiode, a series of spectra were acquired with each spectrum shifted prior to acquisition by 0.5 eV relative to the previous spectrum, which is not equal to the interdiode spacing. The resulting spectra were realigned before being added together. The backgrounds were fitted using power-law functions and subtracted from raw data, and multiple scattering intensities removed using the Fourier-ratio method.[12]

III. CALCULATION METHOD

The ground state DOS of NbO_2, MoO_2, and WO_2 were calculated using the full potential, linearized augmented plane wave plus local orbital (LAPW+lo) method,[13] using the WIEN2K program.[14] LAPW is a density-functional-based[15] electronic structure method, which refines the electron density iteratively by solving the Kohn-Sham equations.[16] For the exchange-correlation poten-

tial, the generalized gradient approximation is employed.[17] In the calculations, the radii of the muffin-tin spheres are 2.0 a.u. for transition metal atoms and 1.7 a.u. for oxygen. To save computation time, cutoffs of $RK_{max}=6.0$ and 2000 k points in the irreducible zone were used. It was found that these conditions are sufficient for the reproduction of experimental ELNES with poor energy resolution (>1 ev). All calculations use experimental measurements of lattice constants and atomic positions for NbO_2,[18] MoO_2,[19] and WO_2.[20] No structural relaxation was performed.

At room temperature, NbO_2 is tetragonal with space group $I4_1/a$. The lattice parameters are $a=13.696$ and $c=5.981$ Å. Both MoO_2 and WO_2 have the same structure: monoclinic, space group $P2_1/c$. The lattice parameters are $a=5.611$, $b=4.856$, $c=5.629$ Å with $\beta=120.95°$ for MoO_2, and $a=5.563$, $b=4.896$, $c=5.663$ Å with $\beta=120.47°$ for WO_2. Although the Bravis lattices are different among these dioxides, their local environments are all related to tetragonal rutile TiO_2.[21] In the rutile structure, each metal atom is octahedrally coordinated to six oxygen atoms. Along the rutile c axis, the edge-sharing oxygen octahedra form chains, which are interlinked via oxygen corners. The symmetry of the octahedron is not perfect; it either extends or shortens along the apical axis. Therefore, there exist two different M-O distances: two apical and four equatorial distances. Figure 1(a) is a plan view of rutile down $(\bar{1}10)$ [given in Fig. 1(c)], which schematically shows part of the chain of edge-sharing MO_6 octahedra in the rutile structure. The metal atoms are equally spaced along the rutile c axis. Each oxygen atom is surrounded by three metal atoms in a planar geometry; two are equatorial and one is apical. In the structures of NbO_2, MoO_2, and WO_2, which are considered as the distorted rutile, the metal-metal distances alternate along octahedral chains. As a result transition metal atoms form pairs along the rutile c axis. Part of the chain of edge-sharing MO_6 octahedra in the distorted rutile is schematically shown in Fig. 1(b). The oxygen octahedra are highly distorted in these structures. It is seen that metal-metal pairing also causes the oxygen surroundings to change, and thus lifts the oxygen into two inequivalent sites (indicated as O1 and O2 in Fig. 1). Although there are four inequivalent oxygen sites in an NbO_2 unit cell, they can be approximately categorized into two groups. The geometric parameters indicated in Fig. 1(b) for NbO_2, MoO_2, and WO_2 are listed in Table I. The octahedral chains (i.e., rutile c axis) lie along the **c** direction of the NbO_2 lattice and the **a** direction in MoO_2 and WO_2.

In order to understand the O K ELNES in these dioxides, calculations have also been carried out for their regular rutile forms. NbO_2 undergoes an apparently second-order transition from the low-temperature tetragonal phase to the high-temperature regular rutile form [$a^R=4.85$, $c^R=3.03$ Å, and $u=0.2925$ (Ref. 22)] at $\sim 810°$C. The structural relationship between tetragonal (T) and rutile (R) NbO_2 can be viewed as $[100]_T \| [110]_R$, $[010]_T \| [\bar{1}10]_R$, and $[001]_T \| [001]_R$. On the contrary, no rutile forms have been reported for MoO_2 and WO_2. Therefore, the hypothetical rutile cell for MoO_2 ($a^R=4.856$, $c^R=2.805$ Å, and $u=0.2847$) constructed by Eyert *et al.*[6] is used in this work. Using the same method for $a^R=b/2$ and $c^R=a$ (Ref. 6), the hypothetical rutile cell for WO_2 ($a^R=4.8963$ and $c^R=2.7815$ Å) was also constructed and used in this work. Since WO_2 and MoO_2 are isostructural, with similar oxygen positions, we use the same internal parameter $u=0.2847$ for WO_2.

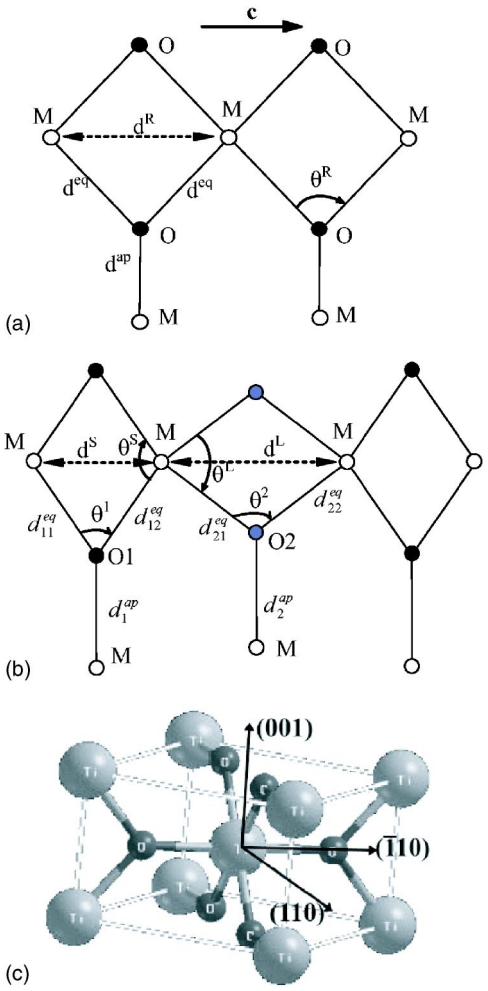

FIG. 1. Schematic drawings of (a) regular and (b) distorted rutile structure on the base plane. M and O represent transition metal and oxygen, respectively. The arrow marked by c indicates the rutile c axis. (c) is the unit cell of rutile TiO_2.

IV. RESULTS

A. NbO_2

Experimental EELS of the O K edge of NbO_2 is given in Fig. 2 (thick solid line). Overall, five major peaks marked a, b, c, d, and e can be recognized in the spectrum. The first three peaks (a, b, and c) are within the first 20 eV from the ionization threshold. The last two broad peaks (d and e) are beyond 20 eV from the threshold. The energy positions of all these peaks are listed in Table II. Broadly speaking, details within the 20 eV range from the threshold can be considered as near-edge fine structure, i.e., O K ELNES. It is known that the ELNES not only depends on the local coordination, but also on the bonding distances and angles. Beyond 20 eV, the features are generally broad, and are considered to be extended fine structure, which will not be discussed in detail in

TABLE I. A list of geometry parameters of distorted rutile structures for NbO_2, MoO_2 and WO_2. The geometries are given in Fig. 1. For comparison, the corresponding parameters of regular rutile structure are also given.

	O1−*M*				O2−*M*			
	d_{11}^{eq}	d_{12}^{eq}	d_1^{ap}	θ^1	d_{21}^{eq}	d_{22}^{eq}	d_2^{ap}	θ^2
NbO_2	2.043	2.056	2.030	84.06°	2.102	2.175	1.934	99.12°
MoO_2	1.984	1.995	1.972	78.22°	2.065	2.073	1.977	97.54°
WO_2	1.969	2.020	1.975	76.71°	2.061	2.108	1.989	95.90°
	M-M				Rutile			
	d^S	θ^S	d^L	θ^L	d^R	θ^R		
NbO_2	2.743	95.85°	3.256	80.83°	2.993	95.05°		
MoO_2	2.510	101.78°	3.112	82.46°	2.805	86.98°		
WO_2	2.475	103.29°	3.096	84.10°	2.782	86.02°		

this work. It is seen that beside these strong peaks, the O *K* ELNES also shows some other weak fine structure. On the high-energy side of peak *b*, a shoulderlike feature is indicated by an arrow (marked as *s*). Between peak *b* and peak *c*, there is a small bump. A shoulder is also seen on the tail of peak *c*.

In Fig. 1, the calculated oxygen *p* DOS is compared with the experimental O *K* ELNES of NbO_2. The theoretical results have been aligned with the position of peak *a*. It should be noted that no core-hole effect and no atomic transition background are considered in the calculations, and the results have been broadened to 1.0 eV using a Gaussian function, to match the experimental broadening. Remarkably, the calculation in the tetragonal (distorted rutile form) NbO_2 (thin solid line) fits the experiment very well: not only the energy positions of the five strong peaks, but also their relative intensities. The weak fine structure in the near-edge range is also reproduced: a shoulderlike feature on the tail of peak *b*, a small bump between peak *b* and peak *c* and a shoulder on the tail of peak *c*. Quantitatively, however, there are some discrepancies. The calculated intensity of peak *a* relative to that of peak *b* is too strong in comparison with the experiment. Additionally, the intensity of small bump between peak *b* and peak *c* is also weaker than the experimental observation. These may be due to the assumptions in the calculations, such as the many-body effects and exchange-correlation potentials. However, further investigation is needed to clarify this.

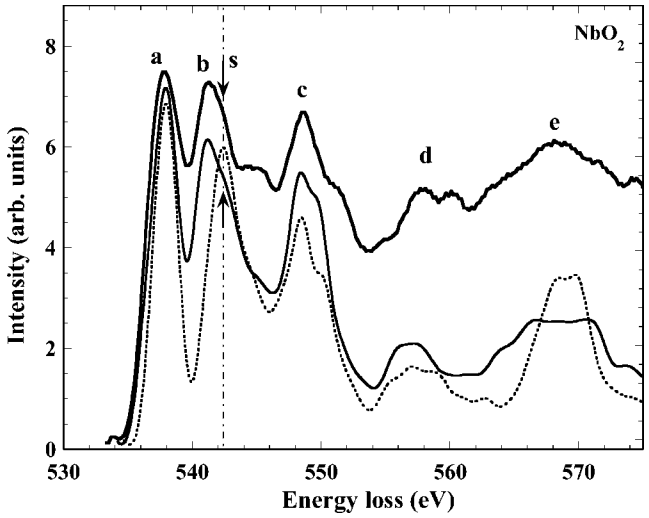

FIG. 2. Comparison of experimental EELS (thick solid line) of the O *K* edge in NbO_2 with calculations. The calculations were carried out in both tetragonal (thin solid line) and rutile structure (dotted line).

Our calculation of the idealized rutile form (dotted line in Fig. 1) also shows the five strong peaks, and the shoulder on the tail of peak *c*, but it does not reproduce the weak features: peak *b* is rather symmetric without the shoulderlike feature, and a small bump between peak *b* and *c* is missing. In the idealized rutile form, NbO_2 shows a 4.4 eV splitting between peak *a* and peak *b*, which is much wider than the 3.2 eV splitting in the distorted form. The corresponding experimental value is close to the latter, which is about 3.5 eV. All these differences are probably due to changes in bond distances and angles, and will be discussed in the next section.

B. MoO_2

Figure 3 shows the EELS of the O *K* edge of MoO_2 (thick solid line). The energy positions of these peaks are listed in Table II. As for NbO_2, five strong peaks can be identified. There are also differences: peak *a* is narrow and the splitting of peaks *a* and *b* is small in MoO_2 in comparison with NbO_2. We also note that peak *b* is asymmetric: a shoulderlike fea-

TABLE II. Energy-loss values for the O *K* ELNES shown in Figs. 2–4.

	a	*b*	*c*	*d*	*e*
NbO_2	537.8	541.3	548.7	558.0	568.3
MoO_2	532.0	535.0	544.1	553.3	564.6
WO_2	533.2	536.9	544.1	553.6	566.2

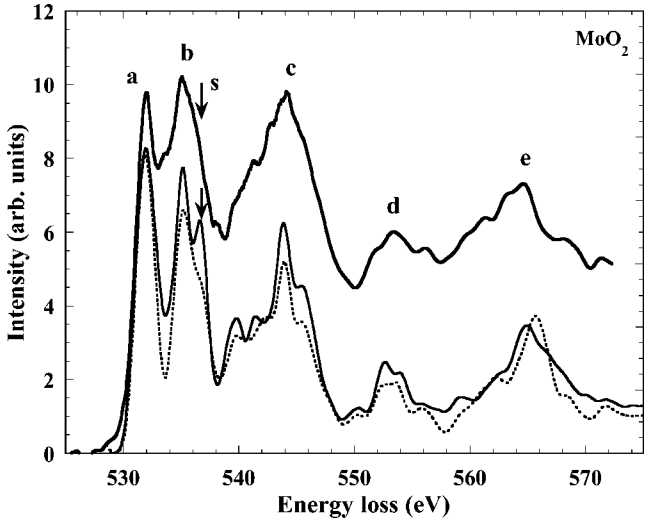

FIG. 3. Comparison of experimental EELS (thick solid line) of the O *K* edge in MoO_2 with calculations. The calculations were carried out in both tetragonal (thin solid line) and rutile structure (dotted line).

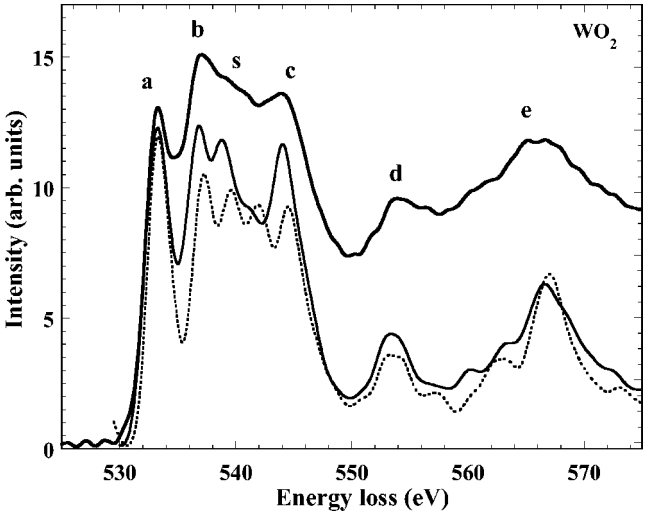

FIG. 4. Comparison of experimental EELS (thick solid line) of the O *K* edge in WO_2 with calculations. The calculations were carried out in both tetragonal (thin solid line) and rutile structure (dotted line).

ture on the high-energy side of peak *b* is more significant (indicated by an arrow in Fig. 3) by comparison with that of NbO_2. Instead of the small bump between peak *b* and peak *c* observed in NbO_2, the corresponding feature in MoO_2 becomes more intense, which results in a very broad peak *c*.

For comparison, the calculated oxygen *p*-DOS of MoO_2 in both monoclinic (thin solid line) and idealized rutile (dotted line) have been aligned to the position of peak *a* of the experiment, and plotted in Fig. 3. Remarkably, the calculation of the monoclinic (distorted rutile form) MoO_2 matches the experiment very well, except for the relative intensity of peak *a*. Contrary to NbO_2, the differences are small in the calculations between the monoclinic and idealized rutile of MoO_2. However, a significant change of intensity indicated by an arrow is observed: a small peak occurs in the distorted rutile form, which decreases to a shoulder in the hypothetical rutile form. This small peak is responsible for the significant shoulderlike feature in the experiment.

C. WO_2

Figure 4 shows the EELS of the O *K* edge of WO_2 (thick solid line). Overall, five peaks can also be recognized, although peaks *b* and *c* largely overlap and form a rather broad feature. The broad feature consists of the strong peak *b* followed by a shoulderlike feature and weak peak *c*. The splitting of peak *a* and peak *b* is larger in WO_2 than in MoO_2 although they have the same structure and same *d* electron configuration.

The calculated O *p* DOS in both monoclinic (thin solid line) and idealized (dotted line) rutile forms are also compared in Fig. 4. The calculation of the monoclinic (distorted rutile) WO_2 fits the experiment very well. All the features, including the overlap of peaks *b* and *c*, can be reproduced except the relative intensity of peak *a*. Due to the overlap, the shoulderlike feature on peak *b* and the bump on peak *c*, which are observed in both NbO_2 and MoO_2, cannot be resolved in WO_2. The calculation of the idealized rutile form gives the four-peak features of the broad peak, and each peak has similar intensity.

V. DISCUSSION

In NbO_2, MoO_2, and WO_2, EELS of the O *K* edge show the same underlying structure. The interpretation of these five basic peaks can be obtained with the aid of the well-studied rutile structure TiO_2.[23] The same five-peak features were also observed in rutile TiO_2 in our previous work[24] and by other researchers. This is probably because these transition metal dioxides have similar local structures to TiO_2, although their long-range order is different. Fortunately, DOS and thus ELNES are determined by the local environment rather than long-range order.[25] In the octahedron of idealized rutile, the transition metal *d* states split into two parts: t_{2g} and e_g, which involve *M*-O π and σ bonding and antibonding interactions, respectively. Accordingly, the first two peaks (*a* and *b*) are due to oxygen *p* states hybridized with the transition metal t_{2g} and e_g states, and thus assigned as t_{2g} and e_g peaks, respectively. The spacing between peak *a* and *b* is a measure of the ligand-field splitting of the t_{2g} and e_g states of the oxygen octahedron.

The justification of these assignments is confirmed by the DFT-LDA calculations. As an example, Fig. 5 shows a comparison of the unoccupied partial DOS for tetragonal and rutile NbO_2. It is noted that the calculation predicts a small band gap ($\sim$0.15 eV) in tetragonal NbO_2, although it is much smaller than the experiment value ($\sim$0.5 eV).[26] The Nb 4*d* states almost completely split into t_{2g} ($-1.0-3.5$ eV) and e_g (3.5−8.0 eV) groups of bands. The small t_{2g}-e_g configuration mixing is due to the distortion of octahedra. The Nb $d_{3z^2-r^2}$ orbital points in the rutile *c* direction, and also belongs to t_{2g} in the ideal rutile structure. However, in distorted rutile NbO_2, the transition metal pairing along the

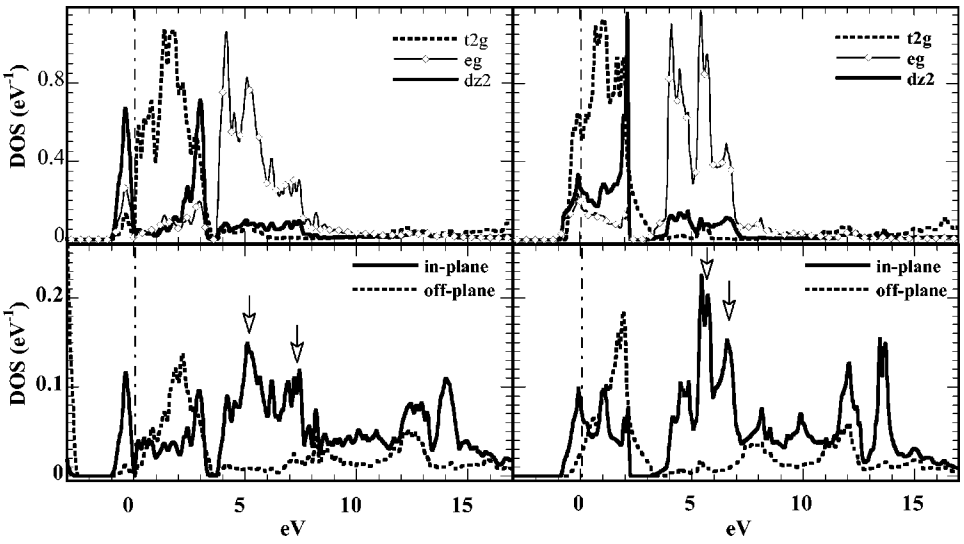

FIG. 5. Comparison of partial DOS of NbO_2 in tetragonal (left panel) and regular rutile (right panel) structure. The chained lines represent Fermi level.

rutile *c* axis significantly changes the $d_{3z^2-r^2}$ band. In idealized rutile, this band has only a weak tendency to split into two peaks, but it completely splits into two peaks at ~ -1.5 and 4.0eV in the distorted rutile structure, allowing the partial DOS to fall to a small value between them. These results are consistent with Goodenough's model, in which the t_{2g} band splits into $d_{\|}$ and π^* bands.[27] The strong *M*-*M* *d*-electron interaction in the distorted rutile structure causes the $d_{\|}$ to further split into bonding and antibonding states. According to this model, the $d_{3z^2-r^2}$ states are designated as the $d_{\|}$ band, with two separated peaks corresponding to *M*-*M* bonding and antibonding states, respectively. The π^* is strongly hybridized with the O $2p\pi$ states, and remains between two $d_{3z^2-r^2}$ peaks.

As shown in Fig. 1, oxygen atoms are coordinated with three metal atoms nearly in a plane in distorted rutile. Therefore, the *M*-*M* pairing, which is perpendicular to the O $2p\pi$ orbital, has little effect on the O $2p\pi$ DOS (indicated as off-plane in Fig. 5), which bears a similarity to both the idealized and distorted rutile structures. However, the *M*-*M* pairing significantly changes the O $2p\sigma$ DOS (indicated as in-plane in Fig. 5). The strong hybridization with Nb $d_{3z^2-r^2}$ results in the splitting of the O $2p\sigma$ in the range from -1.0 to 3.5 eV. Unfortunately, the energy resolution of our spectrometer is not good enough to resolve the change in the t_{2g} peak in the experiments. In the range from 4.0 to 8.0 eV, the O $2p\sigma$ also splits into two peaks (indicated by arrows), which shows in the experiments (Fig. 2) as a shoulderlike feature in the high-energy side of the e_g peak. However, this splitting does not directly relate to the Nb $d_{3z^2-r^2}$, because it makes little contribution in this energy range.

A reasonable interpretation can be based on changes in the local structural arrangement around oxygen, induced by dimerization in the distorted rutile structure. The *M*-*M* pairing reduces the symmetry around the oxygen, and lifts the oxygen degeneracy into two different sites in general, which are defined as O1 and O2 in Fig. 1. O1 and O2 are associated with the short and long *M*-*M* pair, respectively. The bond angle of *M*-O1-*M* becomes smaller, while that of *M*-O2-*M* increases. Additionally, the average *M*-O1 distance is shorter than that of *M*-O2. The differences in the local structural arrangements alter significantly the partial DOS projected on each of these two oxygen atoms. Figure 6 compares the O *p* DOS on O1 and O2 in NbO_2, MoO_2, and WO_2. The main difference is that the densities on the O1 between 4.0 and 8.0 eV become flat in comparison with those on the O2. This enhances the intensities of the second subpeak (black arrows) of the e_g band relative to the first one (white arrows). In the O *K* ELNES, this is reflected by the appearance of the shoulderlike feature on the high-energy side of the e_g peak.

We also note that the width of the t_{2g} peak of NbO_2 is much larger than that of MoO_2 and WO_2, while the later two are quite similar. This can be understood by considering their

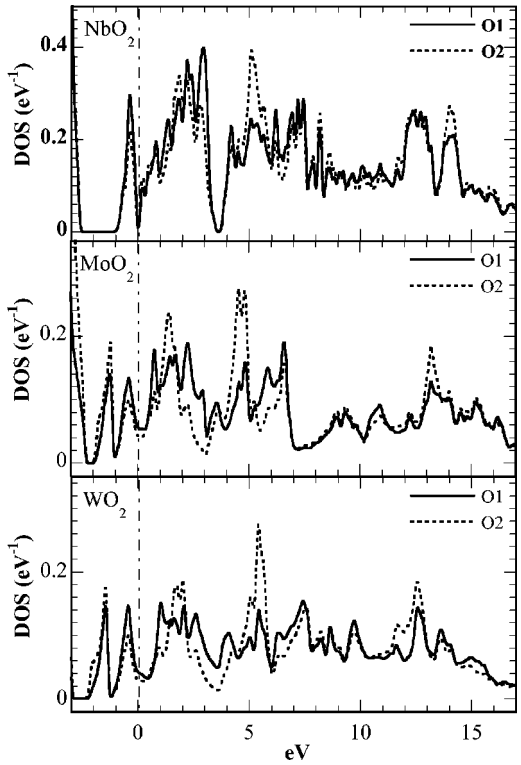

FIG. 6. Comparison of O *p* DOS projected on two different oxygen sites, O1 and O2 in NbO_2, MoO_2, and WO_2. The chained line denotes the Fermi level.

d electron configurations: it is d^1 for NbO_2 but d^2 for MoO_2 and WO_2. One more *d* electron in MoO_2 and WO_2 filling the t_{2g} states narrows down the width of the empty t_{2g} band. In other words, the width of the t_{2g} peak depends on the occupancy of the transition metal *d* electron, and it decreases from $d^0(TiO_2)$, $d^1(NbO_2)$, to d^2 (MoO_2 and WO_2).

Unlike the first two peaks, the origin of the third peak (peak *c*), which varies significantly from oxide to oxide, is not obvious. Usually, it is attributed to the interaction of O 2*p* and transition metal 4*sp* states. However, this assignment, particularly in TiO_2, has been questioned by de Groot *et al.*, because none of Ti 4*s* and 4*p* has maximum intensity in the energy range of peak *c*.[28] Therefore, peak *c* was assigned to antibonding combinations of direct O-O interactions. This assignment is reexamined in this work. Careful inspection of structural details reveals that the O-O bonding distances and corresponding bond angles are very similar to each other in MoO_2 and WO_2. If the O-O interaction had the dominant role, both MoO_2 and WO_2 would have the same appearance as peak *c*. In fact, this peak shows a completely different intensity distribution and energy position in these two isostructural dioxides. Therefore, the O-O interactions may not play a dominate role in these oxides.

According to our calculations, the origin of peak *c* is associated with the appearance of metal *d* states. In both NbO_2 and MoO_2, metal *d* states have relatively strong peaks at same energy as peak *c*. The bumps before peak *c* in these two oxides also relate to the metal states. Interestingly, both NbO_2 and MoO_2 5*s* states, which show narrow and sharp peaks (not shown here), have maxima at the energies where the shoulders are on the high-energy side of peak *c*. This shoulder occurs about 14.3 eV above the threshold in NbO_2, which is close to the calculated 14.1 eV of Nb 5*s* maximum above the Fermi energy. In MoO_2, the corresponding experimental and calculated values are 15.4 and 15.5 eV, respectively. On the contrary, the W 6*s* state in WO_2 shows a broad and dispersive peak in the 5 eV range, instead of a narrow and sharp peak, as in NbO_2 and MoO_2. This is responsible for the broad character of peak *c* in WO_2.

Peak *d* in all three oxides has strong metal *p* character. In the high-energy region, however, it is difficult to relate the broad features to the partial DOS. The appearance of peak *e*, which we do not discuss, has been related to the nearest-neighbor structure.[29]

VI. CONCLUSION

The good fit here between calculation and experiment indicates the accuracy of DFT calculations within the LDA approximation for these transition metal dioxides at our energy resolution. This ground state approach to final state spectra indicates that core-hole effects on O *K* edge in these dioxides have been efficiently screened by the valence electrons.

The O *K* ELNES (empty states, absorption spectra) of NbO_2, MoO_2, and WO_2 have been interpreted here in detail with the aid of band structure calculations. It is found that all the dioxides have the same underlying peak structure in the O *K* ELNES. These peaks reflect the similarity of the local structure of distorted rutile. The small variations in bond distances and angle (or local structural fluctuations), as well as their variations *d* electron configuration, only affect the weak fine structure. In particular, the shoulderlike features observed on the e_g peak have been related to the structural distortion induced by the formation of metal-metal pairs.

ACKNOWLEDGMENTS

This work is supported by NSF Grant No. DMR-0245702. We gratefully acknowledge the use of facilities within the Centre for Solid State Science at Arizona State University.

[1] F. J. Morin, Phys. Rev. Lett. **3**, 34 (1959).
[2] D. B. Rogers, R. D. Shannon, A. W. Sleight, and J. L. Gillson, Inorg. Chem. **8**, 841 (1969).
[3] J. B. Goodenough, Phys. Rev. **117**, 1442 (1960).
[4] N. F. Mott, Philos. Mag. **6**, 287 (1961).
[5] A. Zylbersztejn and N. F. Mott, Phys. Rev. B **11**, 4383 (1975).
[6] V. Eyert, R. Horny, K. -H. Hock, and S. Horn, J. Phys.: Condens. Matter **12**, 4923 (2000).
[7] V. Eyert, Europhys. Lett. **58**, 851 (2002).
[8] V. Eyert, Ann. Phys. (N.Y.) **11**, 650 (2002).
[9] L. L. Chase, Phys. Rev. B **10**, 2226 (1974); M. A. K. L. Dissanayake and L. L. Chase, *ibid.* **18**, 6872 (1978).
[10] F. Werfel and E. Minni, J. Phys. C **16**, 6091 (1983); N. Beatham and A. F. Orchard, J. Electron Spectrosc. Relat. Phenom. **16**, 77 (1979).
[11] P. Rez, J. Bruley, P. Brohan, M. Payne, and L. A. J. Garvie, Ultramicroscopy **59**, 159 (1995).
[12] R. F. Egerton, *Electron Energy-loss Spectroscopy in the Electron Microscope* (Plenum Press, 1996), pp. 302–303.
[13] E. Sjöstedt, L. Nordström, and D. J. Singh, Solid State Commun. **114**, 15 (2000).
[14] P. Blaha, K. Schwarz, G. K. H. Madsen, D. Kvasnicka, and J. Luitz, *WIEN2K, An Augmented Plane Wave + Local Orbitals Program for Calculating Crystal Properties* (Karlheinz Schwarz, Tech. Universität Wien, Austria, 2001).
[15] Hohenberg, H. and Kohn, W., Phys. Rev. **136**, B864 (1964).
[16] Kohn, W. and Sham, L. J., Phys. Rev. **140**, A1133 (1965).
[17] J. P. Perdew, S. Burke, and M. Ernzerhof, Phys. Rev. Lett. **77**, 3865 (1996).
[18] A. K. Cheetham and C. N. R. Rao, Acta Crystallogr., Sect. B: Struct. Crystallogr. Cryst. Chem. **B32**, 1579 (1976).
[19] B. G. Brandt and A. C. Skapski, Acta Chem. Scand. (1947-1973) **21**, 611 (1967).
[20] D. J. Palmer and P. G. Dickens, Acta Crystallogr., Sect. B: Struct. Crystallogr. Cryst. Chem. **B35**, 2199 (1979).
[21] R. Pynn, J. D. Axe, and R. Thomas, Phys. Rev. B **13**, 2965 (1976).
[22] A. A. Bolzan, C. Fong, B. J. Kennedy, and C. J. Howard, Acta

Crystallogr., Sect. B: Struct. Sci. **B53**, 373 (1997).
[23] L. A. Grunes, R. D. Leapman, C. N. Wilker, R. Hoffman, and A. B Kunz, Phys. Rev. B **25**, 7157 (1982).
[24] B. Jiang, J. M. Zuo, N. Jiang, M. O'Keeffe, and J. C. H. Spence, Acta Crystallogr., Sect. A: Found. Crystallogr. **A59**, 341 (2003).
[25] D. Weaire and M. F. Thorpe, Phys. Rev. B **4**, 2508 (1971).
[26] D. Adler, Rev. Mod. Phys. **40**, 714 (1968).
[27] J. B. Goodenough, Prog. Solid State Chem. **3**, 145 (1971).
[28] F. M. F. de Groot, J. Faber, J. J. M. Michiels, M. T. Czyzyk, M. Abbate, and J. C. Fuggle, Phys. Rev. B **48**, 2074 (1993).
[29] H. Kurata, E. Lefever, C. Colliex, and R. Brydson, Phys. Rev. B **47**, 13 763 (1993).